Obrabotka metallov (tekhnologiya, oborudovanie, instrumenty) = Metal Working and Material Science. 2026 vol. 28 no. 2 pp. 136–156
ISSN: 1994-6309 (print) / 2541-819X (online)
DOI: 10.17212/1994-6309-2026-28.2-136-156

NSTU NETI

Obrabotka metallov -
Metal Working and Material Science

Journal homepage: http://journals.nstu.ru/obrabotka_metallov

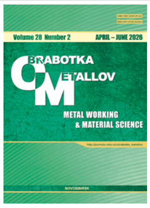

Selection and justification of geometric parameters of the roller contact surface for line-by-line surface plastic deformation

Semen Zaydes [a], ***Thanh Chung Le*** [b, *]

Irkutsk National Research Technical University, 83 Lermontov str., Irkutsk, 664074, Russian Federation

[a] http://orcid.org/0000-0001-9416-7749, zsa@ex.istu.edu; [b] http://orcid.org/0009-0003-2787-1746, lechung275@gmail.com

ARTICLE INFO

Article history:
Received: 03 March 2026
Revised: 16 March 2026
Accepted: 21 March 2026
Available online: 15 June 2026

Keywords:
Surface plastic deformation
Line-by-line processing
Annular roller
Contact surface geometry
Finite element method
Residual stresses
Hardening depth
Microrelief
Controlled deformation constraint
Modified profile

ABSTRACT

Introduction. The paper is devoted to the selection and justification of rational geometric parameters for the contact surface of an annular roller used in line-by-line surface plastic deformation (*SPD*). The relevance of this work stems from the need to enhance the service performance of machine components while ensuring high surface quality and processing productivity. ***The purpose of the study*** is to determine a tool working profile geometry that provides maximum hardening depth and compressive residual stress levels with minimal distortion of the surface microgeometry under conditions of overlapping single deformation tracks. **Methods.** To solve the formulated problem, the finite element method (*FEM*) implemented in the *ANSYS Workbench* software package (Transient Structural module) was employed, using a bilinear isotropic hardening model for *Steel 45* (*AISI 1045*). A comparative analysis of three roller profile types was performed: convex (toroidal), concave (profiled), and straight (cylindrical). During the computational experiment, the tool profile radius and the circular feed step were varied. The efficiency was evaluated based on the criteria of hardened layer depth, residual stress magnitude, and the height of plastic pile-up at the boundaries of adjacent processing tracks. **Results and Discussion.** It is established that the rational profile radius for the toroidal profile is 5.0 mm, and for the profiled roller – 15.5 mm. The disadvantages of the basic geometries are identified: the toroidal roller provides a hardening depth of 1.15 mm but requires small feeds (resulting in low productivity); the profiled roller allows for increased feed, but the hardening depth decreases to 0.91 mm. It is shown that the use of a modified cylindrical profile with fillet transitions enables the effect of “controlled constraint” of plastic deformation. This geometry ensures the formation of a uniform hardened layer with a depth of 1.02 mm, residual stresses of 300–320 MPa, and a micro-irregularity height of 2–5 µm. ***Conclusions.*** The application of the developed tool makes it possible to increase the productivity of the *SPD* process by 5 times compared to the toroidal roller without loss of surface layer quality. The obtained results can be recommended for the design of technological tooling for the finishing and hardening treatment of critical machine components operating under cyclic loads.

For citation: Zaydes S.A., Le T.C. Selection and justification of geometric parameters of the roller contact surface for line-by-line surface plastic deformation. *Obrabotka metallov (tekhnologiya, oborudovanie, instrumenty) = Metal Working and Material Science*, 2026, vol. 28, no. 2, pp. 136–156. DOI: 10.17212/1994-6309-2026-28.2-136-156. (In Russian).

Introduction

Ensuring the operational reliability of critical machine components operating under cyclic loading and wear is inextricably linked to the quality of their surface layer [1, 2]. Among the technological methods aimed at improving fatigue strength and wear resistance, a prominent role is played by finishing and strengthening treatments based on surface plastic deformation (*SPD*) [3, 4]. Traditionally, this technology is implemented using traverse burnishing schemes, in which balls, as well as various types of pin and annular rollers, are widely employed as deforming elements [5]. Among the variety of *SPD* process layouts, line-by-line processing – carried out by the sequential displacement of a local tool-workpiece contact zone

*** Corresponding author**
Le Thanh Chung, Postgraduate Student
Irkutsk National Research Technical University,
83 Lermontov str.,
664074, Irkutsk, Russian Federation
Tel.: +7 950 123-53-82, **e-mail:** lechung275@gmail.com

along a prescribed trajectory – exhibits the highest technological flexibility [6]. A distinctive feature of this method is that the resulting surface characteristics are formed through the discrete overlapping of individual deformation tracks [7].

The efficiency of the line-by-line *SPD* process is governed by the need to achieve a compromise between two competing objectives: maximizing the depth of the hardened layer and the level of compressive residual stresses, which requires high contact pressures, and minimizing residual surface roughness, which necessitates the use of a tool with a smooth contact geometry [8]. A key factor influencing the ability to achieve this balance is the geometry of the roller's working surface. In engineering practice, three basic profile types are commonly used, each characterized by specific features of contact mechanics [9].

However, the direct application of a smooth cylindrical profile (line contact) under line-by-line kinematic conditions is significantly limited due to inevitable edge stress concentration [10]. This geometric feature leads to non-uniform strain hardening and the formation of unacceptable defects in the form of "steps" and material pile-ups in track-overlap regions [11], making it impossible to obtain a high-quality surface without tool modification. On the other hand, a profiled roller with a concave working surface implements enveloping (conformal) contact and contributes to roughness reduction. However, it kinematically induces increased differential sliding at the periphery of the contact patch [12, 13]. This physical effect limits the application of high specific pressures required for deep material hardening.

As an alternative, a toroidal profile forming a localized elliptical contact is considered [14]. This geometry has the potential to minimize edge effects and concentrate the deformation force. Nevertheless, the use of a toroidal roller demands precise coordination of the profile radius with the feed rate, since an arbitrary selection of parameters may lead to pronounced surface waviness in the form of deep residual ridges or dimples, thereby deteriorating surface quality [15].

At the same time, an analysis of the limitations of conventional approaches highlights the necessity of controlling the direction of material flow. In this context, particular importance is attached to implementing the process under conditions of constrained plastic deformation. As shown in [16], the creation of constraint conditions in the contact zone (i.e., restricting the free displacement of material) not only intensifies the hardening process but also significantly improves the homogeneity of the resulting surface layer.

Despite the existence of these fundamental profile types, the scientific and technical literature lacks a comprehensive comparative analysis that would enable a quantitative assessment of their effectiveness specifically under line-by-line processing conditions. This is due to the fact that tools implementing line and enveloping contact in conventional (wide-area) burnishing are technologically unsuitable for line-by-line schemes, as they give rise to surface defects. As a result, uncertainty remains regarding which profile can provide the optimal combination of hardening depth, compressive residual stress level, and residual microrelief quality under identical loading conditions. Without such an analysis, it is difficult to make a substantiated choice regarding the tool's working surface geometry.

The objective of this study is to select and scientifically substantiate the optimal geometric parameters of the contact surface of an annular roller for the line-by-line *SPD* process. To achieve this objective, a multi-criteria problem is addressed: maximizing the depth of hardening and the magnitude of compressive residual stresses while simultaneously minimizing surface microgeometry distortions, specifically the height of plastic pile-ups ($\boldsymbol{h_p}$) formed at the boundaries of single deformation tracks.

Methods

To achieve the stated objective and obtain verifiable data on the microrelief formation mechanism during line-by-line surface plastic deformation (*SPD*), the finite element method (*FEM*) implemented in the *ANSYS Workbench* software package (*Transient Structural* module) was utilized. The *Large Deflection* option was activated in the solver settings, which is a necessary condition for the accurate solution of geometrically nonlinear contact problems involving extensive plasticity [17].

Computational scheme and process kinematics. The physical formulation of the problem is based on the computational scheme illustrated in Fig. 1, *a*. The geometric parameters of the system include a

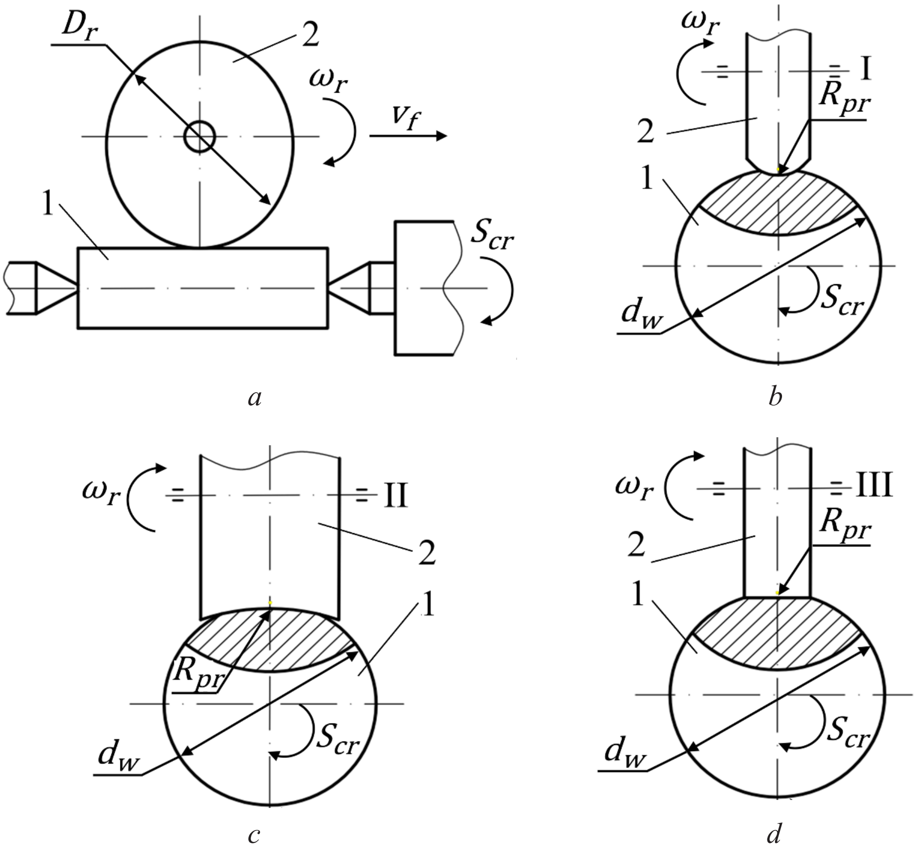

Fig. 1. Geometric and kinematic model of the line-by-line *SPD* process:
a – Schematic diagram of the treatment; *b* – Contact diagram of the roller with a convex working surface (Variant I); *c* – Contact diagram of the roller with a concave working surface (Variant II); *d* – Contact diagram of the roller with a straight working surface (Variant III): **1** – workpiece; **2** – deforming tool

deformable cylindrical workpiece ($\boldsymbol{d_w}$ = 30 mm) and a deforming tool (annular roller) with a diameter of $\boldsymbol{D_r}$ = 40 mm.

A key feature of the study is the modeling of the line-by-line *SPD* kinematics under conditions of rigid kinematic control. The loading cyclogram (see Fig. 1, *a*) is executed via a sequential reciprocating motion scheme, comprising three stages:

– The **radial indentation stage** involves the tool undergoing a forced radial displacement toward the workpiece's longitudinal axis to a fixed depth $\boldsymbol{t}$ (radial interference).

– The **longitudinal deformation stage** involves the tool translating along the workpiece's longitudinal axis at a feed velocity $\boldsymbol{v_f}$. A crucial kinematic condition during this working stroke is the absence of workpiece rotation ($\boldsymbol{\omega_w}$ = 0). The roller's passive rotation about its own axis ($\boldsymbol{\omega_r}$) is induced by friction forces.

– The **circumferential indexing stage** occurs upon completion of the longitudinal stroke. A discrete rotation of the workpiece is executed by the circumferential feed step $\boldsymbol{S_{cr}}$. Following this indexing, the direction of the velocity vector $\boldsymbol{v_f}$ is reversed to perform the working stroke along the subsequent trajectory.

To evaluate the influence of the tool's working profile geometry on the deformation mechanics, three design variants of the deforming roller are investigated (Fig. 1, *b*–*d*). All evaluated tools are bodies of revolution that differ exclusively in the geometry of their working surface generatrix:

Variant I is a roller with a convex working surface (toroidal profile, Fig. 1, *b*). It is characterized by a local (quasi-point) contact, which generates maximum pressure concentration at the center of the deformation zone.

Variant II is a roller with a concave working surface (profiled roller, Fig. 1, *c*). It provides an enveloping (conformal) contact that maximizes the interaction area and restricts lateral material flow (constrained deformation effect).

Variant III is a roller with a straight working surface (cylindrical profile, Fig. 1, *d*). It is characterized by line contact, which theoretically allows for an increase in the circumferential feed step $\boldsymbol{S_{cr}}$ to explore the potential for enhancing hardening productivity.

Finite element model and boundary conditions. The numerical implementation of the problem is based on a three-dimensional solid model. Fig. 2 presents the computational scheme for a roller with a convex working surface (Variant I) as an example; however, the meshing strategy and boundary condition setup are identical for all investigated tool types.

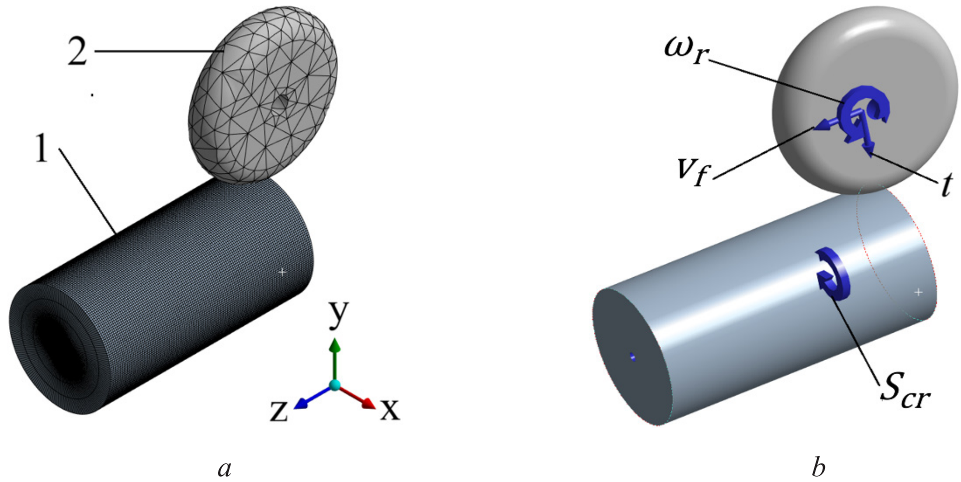

Fig. 2. Finite element model of the process (using a roller with a convex working surface as an example – Variant I):

a – Discretization of the computational domain (hexahedral mesh on the workpiece and tetrahedral mesh on the roller); *b* – Boundary conditions using a Body-Ground joint

To discretize the deformable workpiece, 20-node higher-order hexahedral solid elements of the *SOLID186* type were employed. In the contact interaction zone, local mesh refinement to a characteristic element size of 0.2 mm was applied, which is essential for the accurate resolution of high stress gradients [18]. The deforming tool (roller), treated as a perfectly rigid body, was meshed with tetrahedral elements (Fig. 2, *a*).

The boundary condition system (Fig. 2, *b*) accurately reproduces the prescribed kinematic loading cycle of the process (see Fig. 1, *a*). Workpiece positioning is modeled using a *Body-Ground Joint*, which constrains translational degrees of freedom while permitting the rotation required to implement the circumferential feed ($\boldsymbol{S_{cr}}$). Tool motion is controlled via a *Reference Point* associated with its center of mass. The corresponding kinematic constraints are applied to this point, enforcing radial penetration to a depth $\boldsymbol{t}$ and longitudinal feed at a velocity $\boldsymbol{v_f}$, in accordance with the prescribed processing stages.

Material properties and computational experiment plan. The elastoplastic behavior of the workpiece material (structural carbon steel grade 45, equivalent to *AISI 1045*) was modeled using the *Bilinear Isotropic Hardening* constitutive law. The following material properties were incorporated into the computational scheme: *Young's* modulus $\boldsymbol{E} = 2\times10^5$ MPa, *Poisson's* ratio $\boldsymbol{\mu} = 0.3$, yield strength $\boldsymbol{\sigma_y} = 360$ MPa, and tangent modulus $\boldsymbol{E_t} = 1{,}450$ MPa. The deforming tool was modeled as a rigid body [19].

The computational experiment was designed to conduct a comparative analysis of the effectiveness of various tool profile geometries. To this end, the geometric and kinematic process parameters were divided into fixed parameters (Table 1), which remained constant across all simulation cases, and variable parameters (Table 2), which were systematically varied to evaluate their influence on the resulting surface layer quality characteristics.

Stress State Evaluation Criteria. For a comprehensive quantitative assessment of the stress–strain state (*SSS*) of the processed workpiece, the distortion energy criterion (*von Mises* criterion) was employed. The equivalent stresses during loading and the residual equivalent stresses $\left(\boldsymbol{\sigma_{eq}} \text{ and } \boldsymbol{\sigma_{eq}^{res}}\right)$ were calculated

Table 1

Fixed geometric and processing parameters of the *SPD* process

Parameter	Designation	Value
Workpiece diameter	d_w	30 mm
Roller outer diameter	D_t	40 mm
Depth of penetration (interference)	t	0.1 mm
Longitudinal feed rate	V_l	50 mm/s
Coulomb friction coefficient	f	0.1

Table 2

Variable parameters of the working tool geometry

Tool type (Variant)	Variable parameter	Research objective (Justification)
Variant I. Roller with convex working surface	Profile radius: $\boldsymbol{R_{pr}}$ = 2, 5, 7.5 mm	Optimization search: balance between hardening depth and compressive residual stress magnitude (at small $\boldsymbol{R_{pr}}$) and microrelief quality (at large $\boldsymbol{R_{pr}}$)
Variant II. Roller with concave working surface	Profile radius: $\boldsymbol{R_{pr}}$ = 15.5...16.0 mm	Conformity analysis: evaluation of the effect of the degree of wrap (approximation of $\boldsymbol{R_{pr}} \approx \boldsymbol{R_w}$) on pressure distribution and elimination of edge jamming
Variant III. Roller with straight (cylindrical) working surface	1. Smooth (baseline) 2. Modified (with fillets, side section inclination angle $\boldsymbol{\alpha}$ = 1, and radial reduction $\boldsymbol{\Delta h}$ = 0.05 mm)	Evaluation of modification effectiveness: comparative analysis of the ability of fillet transitions to suppress edge metal pile-up and reduce stress concentration

based on the three principal components of the stress tensor in a cylindrical coordinate system: axial ($\boldsymbol{\sigma_z}$), radial ($\boldsymbol{\sigma_r}$), and circumferential ($\boldsymbol{\sigma_\theta}$) [20]. The equivalent stress during loading is defined by the following expression:

$$\sigma_{eq} = \sqrt{\frac{1}{2}\left[(\sigma_r - \sigma_\theta)^2 + (\sigma_\theta - \sigma_z)^2 + (\sigma_z - \sigma_r)^2\right]}. \quad (1)$$

A similar relationship is used for the residual stresses:

$$\sigma_{eq}^{res} = \sqrt{\frac{1}{2}\left[\left(\sigma_r^{res} - \sigma_\theta^{res}\right)^2 + \left(\sigma_\theta^{res} - \sigma_z^{res}\right)^2 + \left(\sigma_z^{res} - \sigma_r^{res}\right)^2\right]}. \quad (2)$$

In addition to the stress state analysis, an important criterion for evaluating the processing quality is the geometric condition of the resulting microrelief. In this study, the metal pile-up height ($\boldsymbol{h_p}$) is adopted as the primary geometric parameter – defined as the maximum deviation of the surface microprofile above the initial workpiece surface, arising from the plastic flow of material from the central contact zone toward its periphery [21].

Results and discussion

Selection and justification of the parameters for a roller with a convex working surface (Variant I). Fig. 3 presents the contour plots obtained from the numerical simulation, illustrating the distribution of the residual equivalent stress $\left(\boldsymbol{\sigma_{eq}^{res}}\right)$ in the surface layer of the workpieces. Analysis of the obtained results indicates that the roller profile radius ($\boldsymbol{R_{pr}}$) has a decisive influence on the resulting stress state.

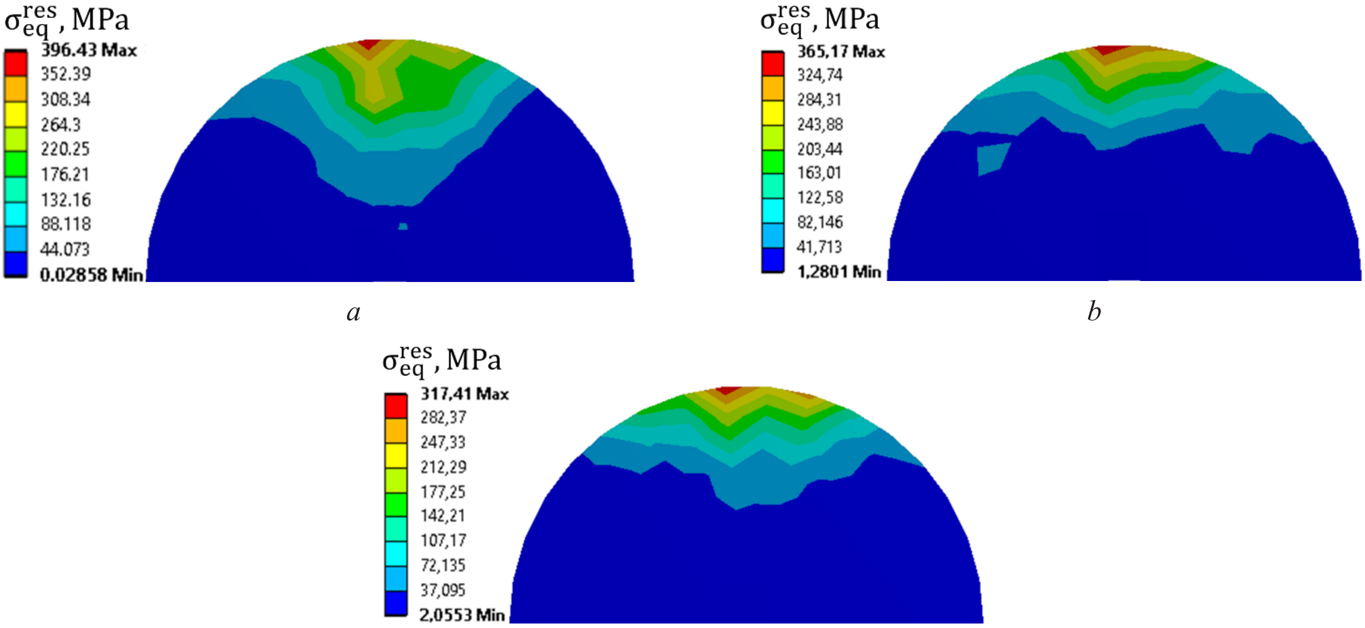

c

Fig. 3. Distribution fields of residual stress magnitude $\left(\sigma_i^{res}\right)$ in the cross-section of the parts at different roller profile radii $\boldsymbol{R_{pr}}$ (Variant I):
a – $\boldsymbol{R_{pr}}$ = 2 mm; *b* – $\boldsymbol{R_{pr}}$ = 5.0 mm; *c* – $\boldsymbol{R_{pr}}$ = 7.5 mm

In particular, at the minimum radius $\boldsymbol{R_{pr}}$ = 2.0 mm (Fig. 3, *a*), the maximum value of the residual equivalent stress is observed, reaching 396.43 MPa. As the radius increases to 5.0 mm (Fig. 3, *b*) and 7.5 mm (Fig. 3, *c*), a consistent reduction in the peak values to 365.17 MPa and 317.41 MPa is observed, respectively.

This trend is governed by contact mechanics: as the profile radius increases, the contact patch expands, leading to load redistribution and a reduction in the specific contact pressure. This behavior is fully consistent with classical *Hertzian* contact theory [22]. Consequently, the equivalent plastic strain decreases, which manifests as a reduction in the residual stress level. Thus, the use of a roller with an excessively small profile radius may result in an extreme stress concentration that significantly exceeds the material's yield strength (for Grade 45 steel: $\boldsymbol{\sigma_y}$ = 360 MPa). This condition is accompanied by excessive work hardening and the subsequent relaxation of residual stresses. Conversely, an excessive increase in $\boldsymbol{R_{pr}}$ causes the stresses to fall below the threshold required for effective surface hardening. For the final verification of the selected geometric parameters of the roller, it is necessary to additionally analyze the geometric characteristics of the surface layer, which are presented in Fig. 4.

Analysis of the graphical dependencies presented in Fig. 4 enabled a highly accurate second-order polynomial approximation of the simulation results, describing the variation in the hardened layer depth $\left(\boldsymbol{h_h} = 0.0012R_{pr}^2 - 0.175R_{pr} + 1.995\right)$ and the pile-up height $\left(\boldsymbol{h_p} = 0.00004R_{pr}^2 + 0.0137R_{pr} + 0.0098\right)$. The observed process dynamics indicate a clear correlation between the investigated parameters: as the profile radius R_{pr} increases from 2.0 to 7.5 mm, a monotonic decrease in the hardening depth from 1.65 to 0.75 mm occurs, accompanied by a simultaneous increase in the plastic pile-up height from 0.013 to 0.022 mm. This trend indicates that with an increase in the tool radius, the processing efficiency declines in terms of both the layer depth criterion and the microgeometry quality.

From a strictly geometric perspective, the regime with the minimum radius ($\boldsymbol{R_{pr}}$ = 2.0 mm) is unconditionally preferable, as it provides the maximum penetration depth into the material with minimal profile distortion ($\boldsymbol{h_p}$ = 0.013 mm). However, a comprehensive verification of this regime based on the stress state criterion (see Fig. 3) revealed its technological unsuitability. At $\boldsymbol{R_{pr}}$ = 2.0 mm, peak residual equivalent stresses of approximately 396 MPa were observed, which significantly exceed the yield strength of

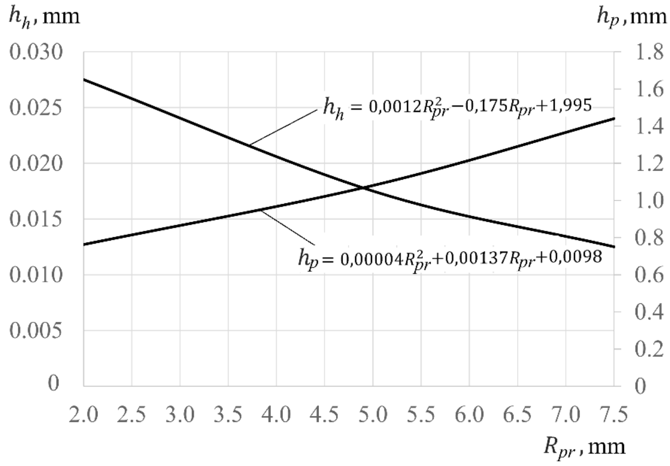

Fig. 4. Effect of the roller profile radius ($\boldsymbol{R_{pr}}$) on the hardened layer depth ($\boldsymbol{h_h}$) and the pile-up height ($\boldsymbol{h_p}$)

Grade 45 steel. Exceeding this threshold initiates stress relaxation and leads to excessive work hardening in the surface layer. The reduction in hardening efficiency in this case indicates the irrationality of using this parameter range, despite its geometric advantages.

To scientifically justify the selection of the optimal roller profile radius, the method of analyzing the intersection of normalized response functions – representing a multi-objective optimization criterion – was applied. This approach enabled a compromise between geometric efficiency and structural reliability. The calculated intersection coordinates revealed a point of "technological equilibrium" corresponding to $\boldsymbol{R_{pr}} \approx 4.8$ mm. This value practically coincides with $\boldsymbol{R_{pr}} = 5.0$ mm, obtained from the numerical simulation and adopted as the baseline parameter. In this regime, the structural integrity of the surface layer is guaranteed by maintaining residual equivalent stresses at a safe level (365.17 MPa), while simultaneously preserving an operationally significant hardening depth ($\boldsymbol{h_h} \approx 1.15$ mm) and keeping the pile-up height within acceptably low limits ($\boldsymbol{h_p} \approx 0.017$ mm).

Analysis of the results presented in Fig. 5 allows determination of the rational range of the circular feed step ($\boldsymbol{S_{cr}}$) during hardening with a convex-profile roller. The primary optimization criteria are the residual ridge height ($\boldsymbol{h_{res}}$), which governs the resulting surface quality, and the number of working passes ($\boldsymbol{N}$), which characterizes process productivity. For small circular feed values ($\boldsymbol{S_{cr}} \leq 0.3$ mm), minimum surface roughness is achieved; however, this is accompanied by a sharp increase in processing effort ($\boldsymbol{N}$ = = 942 passes) and the emergence of a technological risk of excessive work hardening. The most efficient range of circular feeds is $\boldsymbol{S_{cr}} = 0.5$–$0.9$ mm, where a 5- to 8-fold reduction in the number of passes is achieved while maintaining the residual ridge height within technologically acceptable limits ($\boldsymbol{h_{res}} \approx 0.004$–$0.008$ mm).

A further increase in the circular feed step leads to process instability, manifested by a sharp increase in ridge height to 0.062 mm at $\boldsymbol{S_{cr}} = 1.8$ mm. This inflection point can be explained by comparing the circular

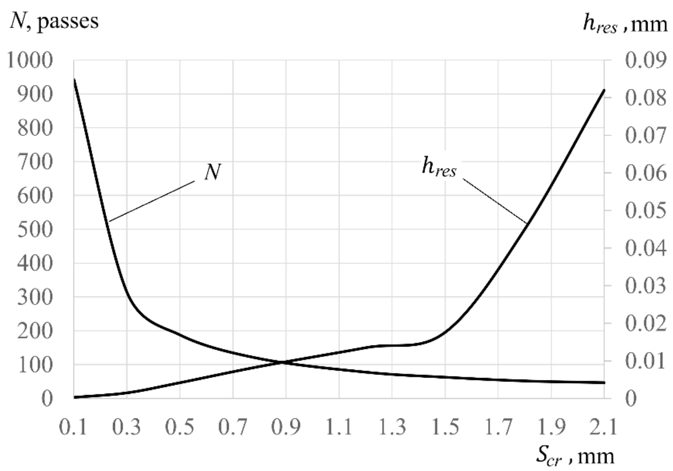

Fig. 5. Effect of the circular feed step ($\boldsymbol{S_{cr}}$) on the residual ridge height ($\boldsymbol{h_{res}}$) and the number of passes $\boldsymbol{N}$ during hardening with a roller with a convex working surface (Variant I)

feed step to the calculated width of a single contact track (***b***). Under the selected processing conditions, the theoretical contact track width, determined from the geometric relation $\boldsymbol{b} \approx 2\sqrt{2tR_wR_{pr} / \left(R_w + R_{pr}\right)}$, is approximately 1.73 mm. Thus, when the circular feed step exceeds this value ($\boldsymbol{S_{cr}} > 1.73$ mm), the step itself becomes the limiting factor, resulting in a loss of processing continuity and the formation of untreated zones. This condition effectively contradicts the kinematic requirement of complete surface coverage. The obtained results demonstrate that the potential for increasing productivity in the toroidal-profile scheme is fundamentally constrained by the track overlap condition. This limitation necessitates the development of alternative deformation schemes with an inherently wider contact zone.

Selection and justification of the parameters for a roller with a concave working surface (Variant II). The transition to a profiled roller (with a concave working surface) is justified by the necessity of implementing conformal (enveloping) contact, enabling a fundamentally different deformation mechanism compared to Variant I. This allows for a significant expansion of the plastic deformation zone. The effectiveness of this scheme is largely determined by the difference between the tool and workpiece radii, $\boldsymbol{\Delta R} = R_{pr} - R_w$. This geometric parameter is the key factor regulating the nature of the surface interaction: ranging from full-profile envelopment at minimal values to a transformation into quasi-point contact as the radii difference increases. The regime where $R_{pr} \le R_w$ is considered technically unacceptable due to the inevitable gouging of the tool edges into the workpiece surface, causing mechanical destruction of the structure.

Analysis of the equivalent stress during loading ($\boldsymbol{\sigma_{eq}}$) distribution (Fig. 6) revealed that at the minimum radii difference $\boldsymbol{\Delta R}$ = 0.5 mm ($\boldsymbol{R_{pr}}$ = 15.5 mm, Fig. 6, *a*), a critical stress concentration emerges, reaching 820.96 MPa (the maximum residual equivalent stress $\boldsymbol{\sigma_{eq}^{res}}$ under these conditions is 311 MPa). This value significantly exceeds the ultimate tensile strength of steel *Grade 45* ($\boldsymbol{\sigma_u}$ = 600 MPa), which is physically explained by the severe constraint on elastoplastic deformation under conditions of high conformity. In this state, the metal, confined within the enclosed space of the concave profile, is unable to flow laterally. This condition leads to a triaxial compressive stress state with a pronounced hydrostatic component, which suppresses plastic flow and promotes premature fracture.

Increasing the radii difference to $\boldsymbol{\Delta R}$ = 1.5 mm ($\boldsymbol{R_{pr}}$ = 16.5 mm, Fig. 6, *c*) leads to a reduction in the active stress to 462.78 MPa, and the residual stress to 247 MPa, which effectively negates the advantages

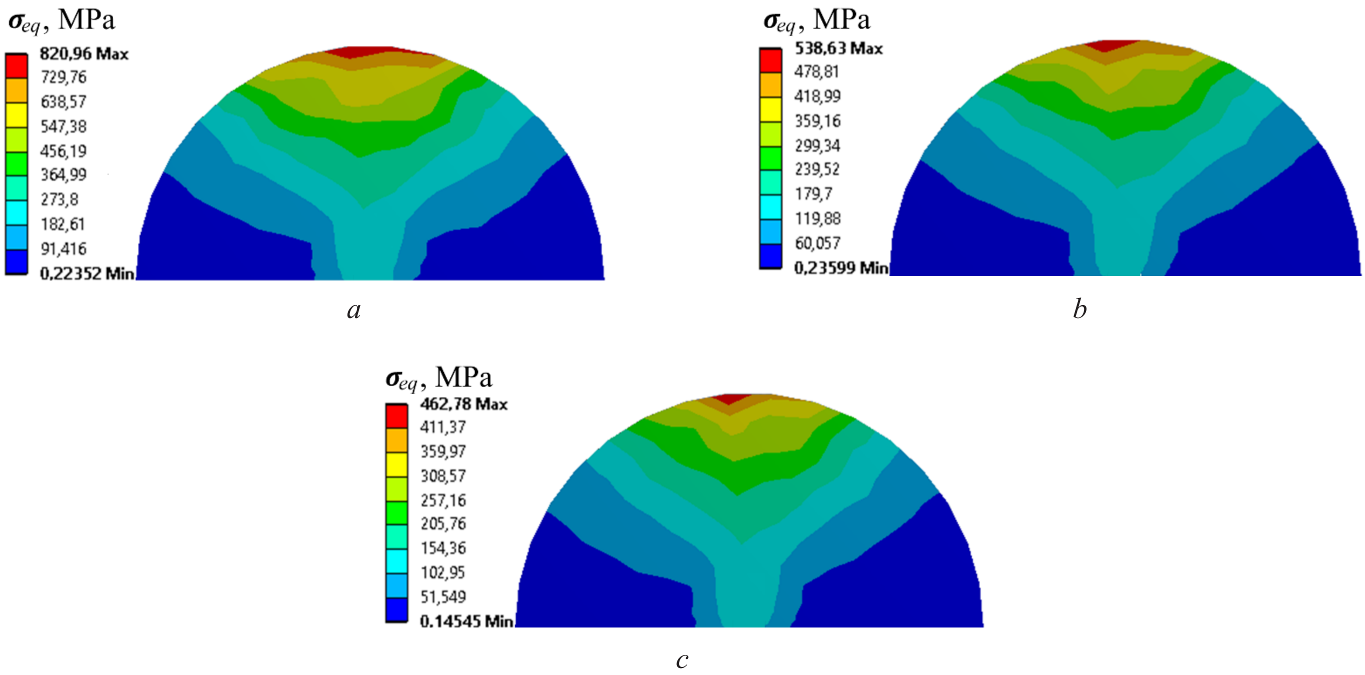

Fig. 6. Distribution fields of transient stress magnitude $\boldsymbol{\sigma_i^{tr}}$ in the deformation zone at different roller profile radii: *a* – $\boldsymbol{R_{pr}}$ = 15.1 mm; *b* – $\boldsymbol{R_{pr}}$ = 15.5 mm; *c*– $\boldsymbol{R_{pr}}$ = 16.0 mm

of conformal contact due to the transition toward a localized (quasi-point) interaction regime. The rational value is established at ΔR = 1.0 mm (R_{pr} = 16.0 mm, Fig. 6, *b*). At this value, the level of equivalent stress during loading (538.63 MPa) is sufficient for the intensive progression of plastic deformation (forming residual stresses of approximately 270 MPa), yet remains within a safe range, eliminating the risk of material fracture.

The preliminary analysis of the stress state highlights the radius R_{pr} = 16.0 mm as the most effective for hardening workpieces with a diameter of 30 mm. For the final verification of this selection, in addition to analyzing the active stress, it is necessary to evaluate the influence of the profile radius on the key characteristics of the formed layer: the hardening depth (h_h) and the pile-up height (h_p). The simulation results for these parameters are presented as graphical dependencies in Fig. 7.

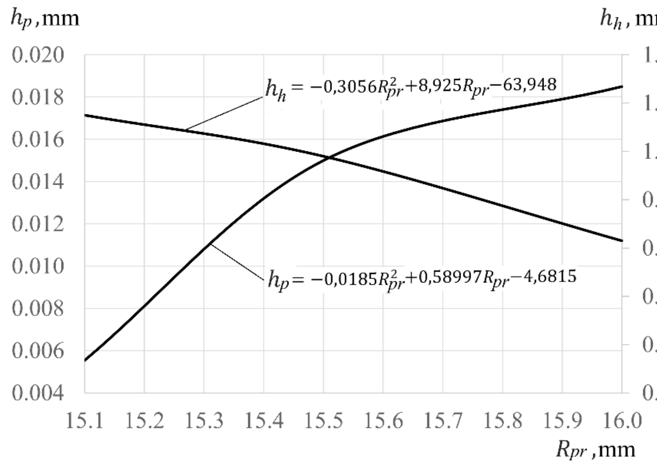

Fig. 7. Effect of the roller profile radius (R_{pr}) on the hardening depth (h_h) and the pile-up height (h_p)

Analysis of the graphical dependencies presented in Fig. 7 and approximated by second-order polynomials $\left(h_h = -0.3056R_{pr}^2 - 8.925R_{pr} - 63.948;\ h_p = -0.0185R_{pr}^2 + 0.590.175R_{pr} - 4.6815\right)$ demonstrates the high sensitivity of the process to changes in the contact geometry. Unlike the convex roller, increasing the radius R_{pr} from 15.1 to 16.0 mm here results in a simultaneous degradation of both quality indicators: the hardened layer depth (h_h) drops abruptly by nearly half (from 1.18 to 0.65 mm), while the pile-up height (h_p) increases from 0.006 to 0.018 mm. From a purely geometric point of view, the regime with the minimum radius (R_{pr} = 15.1 mm) is undoubtedly optimal, providing maximum penetration depth with minimal profile distortion.

However, verification of this regime against the criterion of equivalent stress during loading (σ_{eq}) (see Fig. 6) reveals its technological infeasibility: the emerging maximum stress (820.96 MPa) significantly exceeds the ultimate tensile strength of the material. To resolve this contradiction, the method of analyzing the intersection of normalized functions was utilized, analogous to the approach applied for Fig. 4. Based on this approach, the rational compromise point – representing an optimal balance between deformation intensity and structural integrity – was determined as R_{pr} = 16.0 mm. This selection allows the process to move away from the fracture zone, reducing the active stress to a safe level (538.63 MPa), while simultaneously maintaining high surface layer quality indicators: the residual equivalent stress is formed at 270 MPa, the hardening depth is maintained at $h_h \approx 0.91$ mm, and the pile-up height does not exceed 0.015 mm.

As justified previously, at the rational profile radius R_{pr} = 16.0 mm, the pile-up height (h_p) is minimized due to the conformal contact effect. This creates favorable prerequisites for the processing operation, as the small volume of metal displaced to the sides of the contact zone allows for a significant increase in the circular feed step (S_{cr}) without an abrupt increase in the residual ridge height (h_{res}) during the overlapping of deformation tracks. To scientifically justify the feasibility of applying high circular feeds, it is necessary to evaluate the theoretical contact track width (***b***). With the selected parameters (R_{pr} = 15.5 mm,

$\boldsymbol{R_w}$ = 15.0 mm) and an interference depth $\boldsymbol{t}$ = 0.1 mm, the contact patch width is determined by the following geometric relationship:

$$b \approx 2\sqrt{\frac{2tR_w R_{pr}}{R_{pr} - R_w}} \approx 2\sqrt{\frac{2 \times 0.1 \times 15 \times 15.5}{15.5 - 15}} \approx 19.3 \text{ mm.}$$

This value exceeds the circular feed step by an order of magnitude, ensuring complete overlap of deformation tracks even at elevated feed rates. To test this hypothesis, simulations were conducted over a wide range of circular feeds $\boldsymbol{S_{cr}}$ = 1.0–4.5 mm. The results regarding the variation in the residual ridge height ($\boldsymbol{h_{res}}$) and the number of working passes (***N***) are presented in Fig. 8.

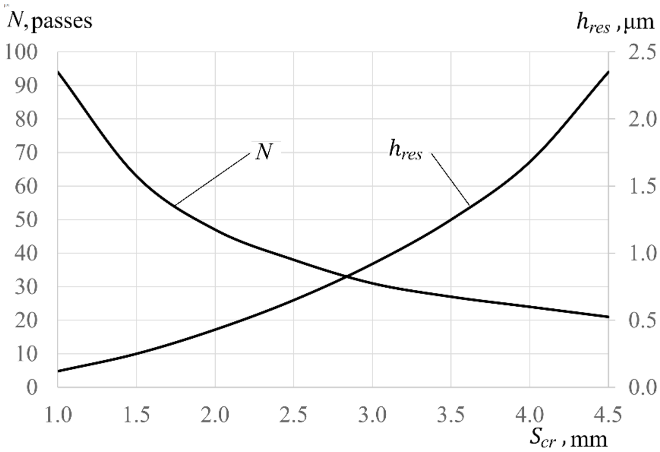

Fig. 8. Dependence of the residual ridge height ($\boldsymbol{h_{res}}$) and the number of passes (*N*) on the circular feed step ($\boldsymbol{S_{cr}}$) during hardening with a concave profile roller

Analysis of the microrelief formation dynamics confirms that, owing to the high geometric conformity between the tool and workpiece profiles, the ridge height between adjacent processing tracks remains minimal even with a significant distance between the feed spirals. This behavior indicates that the kinematic constraint observed in Variant I is effectively eliminated. The simulation results indicate that even when the circular feed is increased to $\boldsymbol{S_{cr}}$ = 3.0 mm, the calculated residual ridge height $\boldsymbol{h_{res}}$ is only about 0.92 μm. This value is substantially lower than the micro-irregularity height characteristic of the toroidal profile operating at a much smaller circular feed ($\boldsymbol{S_{cr}}$ = 1.0 mm). The sharp reduction in the number of working passes ***N*** from 94 to 31 when transitioning to a feed of $\boldsymbol{S_{cr}}$ = 3.0 mm enables a 3-fold reduction in machining time, while keeping the roughness parameters within the requirements for finishing operations. In contrast to the toroidal profile (Variant I), where productivity is limited by the track overlap condition ($\boldsymbol{S_{cr}} \le \boldsymbol{b}$), the conformal scheme enables a substantial increase in feed without compromising surface integrity.

However, the high contact conformity, which ensures superior surface quality and high *SPD* process productivity, also inherently possesses technological limitations. The distribution of the deformation force over a broad contact patch ($\boldsymbol{b}$ ≈ 19.3 mm) leads to a reduction in specific contact pressure compared to the point contact of a toroidal profile. Consequently, the hardened layer depth and the level of accumulated compressive residual stresses are relatively lower when using a profiled roller. This indicates that the selection of a profiled roller is rational in cases where priority is given to productivity and roughness minimization, whereas achieving maximum hardening depth may require alternative design solutions, thereby highlighting the inherent trade-off between productivity and hardening effectiveness in conformal deformation schemes.

Selection and justification of the parameters for a roller with a straight working surface (Variant III). This tool is characterized by line contact (Fig. 1, *d*), which theoretically allows for a significant increase in the circular feed step ($\boldsymbol{S_{cr}}$) to explore the maximum potential for enhancing hardening productivity beyond the limitations identified in Variants I and II. However, in practice, the implementation of a scheme with a straight generatrix is associated with the emergence of pronounced edge effects (stress concentration at the tool ends), which require detailed investigation.

Analysis of the stress-strain state when using a smooth cylindrical profile ($\boldsymbol{D_r}$ = 40 mm, width $\boldsymbol{B}$ = 10 mm) revealed a significant non-uniformity in the force field. The sharp edges of the tool (90°) create a stress singularity, where the peak stresses (830–835 MPa) substantially exceed the ultimate tensile strength of the material [23]. This behavior is characteristic of geometric discontinuities, where the local stress field tends toward theoretically unbounded values. This effect promotes surface micro-fracture and intensive lateral metal flow, leading to the formation of high pile-ups. Meanwhile, in the center of the contact zone, the active stress drops to 550 MPa, forming an undesirable "saddle-shaped" pressure profile (see Fig. 9, *a*). Such a distribution leads to non-uniform plastic deformation and can compromise the integrity of the hardened layer.

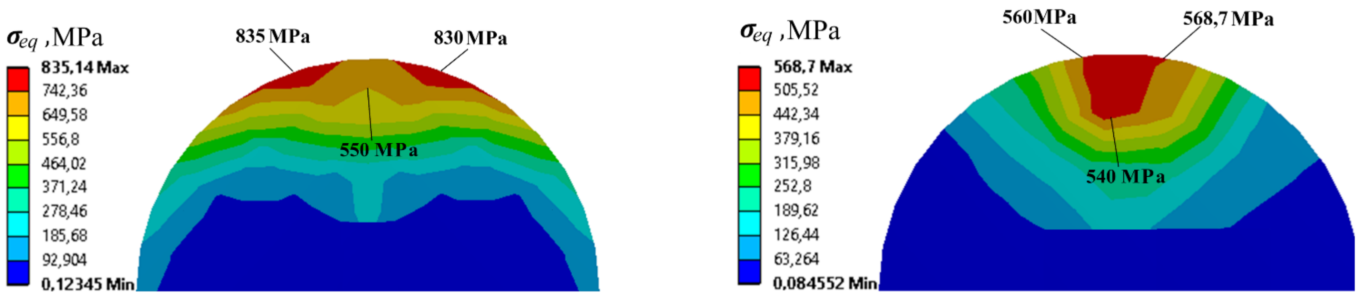

a *b*

Fig. 9. Distribution fields of transient stress magnitude $\left(\,^{tr}\right)$ in the cross-section of the workpiece: (*a*) smooth cylindrical profile; (*b*) modified cylindrical profile

To stabilize the process, a modified cylindrical roller with a width $\boldsymbol{B}$ = 10 mm is proposed; its design parameters are shown in Fig. 10. The tool features a central cylindrical section with a width $\boldsymbol{l}$ = 3 mm, which smoothly transitions via fillets to the side flanks with an inclination angle $\boldsymbol{\alpha}$ = 15° (radial relief $\boldsymbol{\Delta h}$ = 0.05 mm).

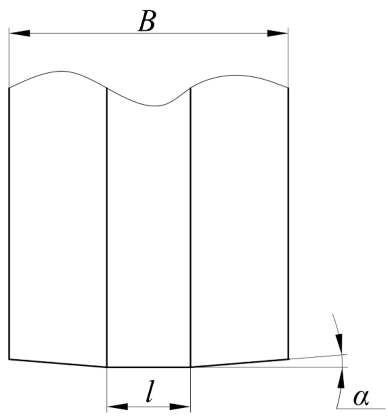

Fig. 10. Design parameters of the modified roller with a central cylindrical section and fillets (α ≈ 1°, $\boldsymbol{\Delta h}$ = 0.05 mm)

These fillet transitions create a controlled constraint effect in the contact zone. By gradually restricting the lateral flow of the metal, they redirect the plastic flow from lateral extrusion to subsurface deformation [24]. As a result, the edge stress peaks are effectively eliminated, and a uniform field of compressive equivalent stresses during loading with optimal values of 540–568.7 MPa is formed in the center (beneath the central cylindrical section) (see Fig. 9, *b*).

The differences in the distribution of the active stresses (see Fig. 9) directly determine the macrogeometry of the deformation zone and the nature of the hardened layer formation. To illustrate the investigated physical and mechanical parameters and their localization in the contact cross-section, calculated surface profiles were plotted, as shown in Fig. 11. The quantitative indicators reflecting the influence of the tool profile on the surface layer quality are summarized in Table 3.

Analysis of the data in Table 3 and the track profiles (see Fig. 11) shows that, owing to the controlled constraint effect, the pile-up height ($\boldsymbol{h_p}$) is reduced by more than 5.5 times – from 37.7 μm to 6.5 μm relative to the baseline tool. Although the peak hardening depth ($\boldsymbol{h_h}$) for the smooth cylindrical profile is slightly higher (1.35 mm), it is characterized by extreme non-uniformity, with a sharp drop to 0.4 mm at the contact center. In turn, the use of the modified profile guarantees the formation of a uniform, rectangular-shaped hardened layer with a depth of 1.015–1.020 mm across the entire width of the processing zone. This transformation from a gradient-type to a quasi-uniform distribution represents a fundamental improvement in surface layer integrity.

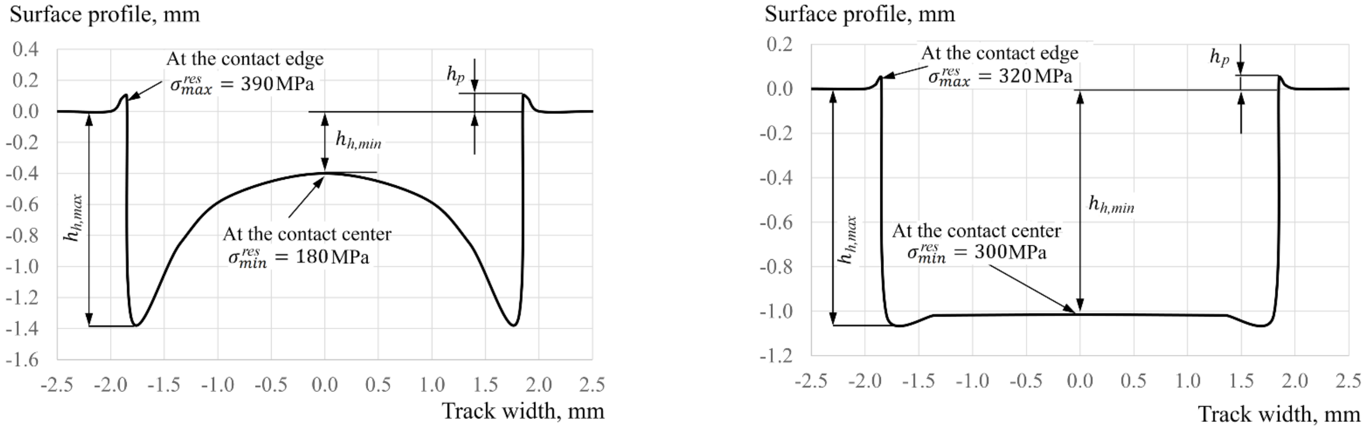

a *b*

Fig. 11. Diagram of the trace profile and localization of the physical and mechanical parameters of the surface layer:

a – smooth cylindrical profile; *b* – modified profile

Table 3

Comparative analysis of the physical and mechanical parameters of the surface layer after hardening by a roller with a smooth cylindrical profile and a modified profile

Parameter group	Parameter localization	Smooth cylindrical profile	Modified profile
h_p	At the edge of the track	37.7 µm	6.5 µm
h_{h_max}	At the edge of contact	1.35 mm	1.02 mm
h_{h_min}	At the center of contact	0.4 mm	1.015 mm
$\left(\sigma_{max}^{res}\right)$	At the edge of contact	390 MPa	320 MPa
$\left(\sigma_{min}^{res}\right)$	At the center of contact	180 MPa	300 MPa

A similar trend is observed in the distribution of residual equivalent stresses $\left(\sigma_{eq}^{res}\right)$: the modified profile provides a stable stress level in the range of 300–320 MPa, whereas the smooth cylindrical profile exhibits a significant value gradient (from 180 to 390 MPa) between the center and the periphery of the contact. Such stability is essential for enhancing fatigue resistance and preventing crack nucleation. Thus, the proposed tool design enables high quality and uniformity in the surface layer state, eliminating dangerous stress concentrators and macrogeometry defects.

The stability of the stress-strain state and the improved track macrogeometry achieved when using the modified profile under single-indentation conditions enable a significant increase in the circular feed step (S_{cr}) without compromising surface quality. When transitioning from the formation of a single track to the continuous processing of a solid surface, the influence of the circular feed step on the output process parameters becomes critical.

As shown in Fig. 12, over a wide range of circular feeds (S_{cr} = 0.5–2.5 mm), the residual ridge height (h_{res}) is maintained at a consistently low level (0.002–0.005 mm) due to the track overlap effect from the central cylindrical section. Concurrently, the number of required working passes (N) is reduced from 189 to 38, confirming the feasibility of achieving high productivity while maintaining the requisite quality. The optimal regime is a circular feed of S_{cr} = 2.5 mm, which ensures maximum process efficiency. A further increase in the feed step beyond 3.0 mm leads to a sharp, sudden increase in h_{res} up to 0.072 mm due to the loss of continuous contact and the breakdown of the track overlap condition. Thus, the proposed filleted

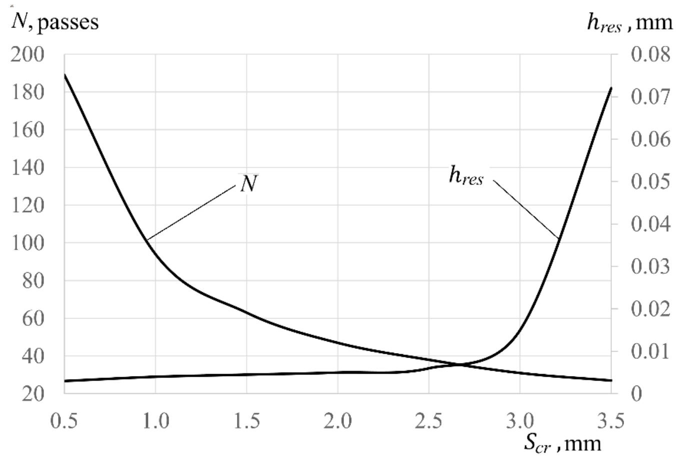

Fig. 12. Effect of the circular feed step (S_{cr}) on the residual ridge height (h_{res}) and the number of passes (N) during processing with a modified profile

roller design enables high-performance deformation under controlled constraint conditions, guaranteeing uniform hardening and minimal roughness.

Comprehensive analysis and theoretical justification of tool contact profiles. A comparative analysis of the technical and economic indicators presented in Table 4 highlights fundamental differences in the mechanics of surface layer formation under different tool–workpiece contact conditions. The use of different roller profiles determines the contact interaction mode – transitioning from point to line contact – which directly affects the stress-strain state of the material in the deformation zone.

Table 4

Summary evaluation of the technical and economic indicators depending on the working tool profile

Indicator	Toroidal (R_{pr} = 5.0 mm)	Profiled (R_{pr} = 15.5 mm)	Modified profile
Circular feed (S_{cr})	0.5 mm	3.0 mm	2.5 mm
Hardening depth (h_h)	1.15 mm	0.91 mm	1.02 mm
Residual stress $\left(\sigma_{max}^{res}\right)$	365 MPa	270 MPa	320 MPa
Surface roughness height (h_{res})	4...8 µm	0.7...1.2 µm	2...5 µm
Number of passes (N)	188	31	38

As shown in Table 4, the application of a toroidal roller (R_{pr} = 5.0 mm) provides the greatest hardening depth (h_h = 1.15 mm) and the maximum level of residual equivalent stresses $\left(\sigma_{eq}^{res} = 365\ \text{MPa}\right)$. However, due to the quasi-point nature of the contact, these extreme values are concentrated exclusively at the center of the deformation zone, resulting in a non-uniform microrelief profile. Furthermore, this approach requires small circular feed steps (S_{cr} = 0.5 mm) to ensure process continuity. This inevitably leads to a significant increase in the number of passes (N = 188) and results in extremely low productivity.

Alternatively, the use of a profiled roller (R_{pr} = 15.5 mm) with conformal contact significantly improves productivity (N = 31 passes) and ensures minimal surface roughness (h_{res} ≈ 0.7–1.2 µm). Nevertheless, the distribution of the deformation force over a significantly larger contact area inevitably reduces the specific contact pressure below the critical threshold required for deep plastic deformation. As a result, the hardening depth decreases to 0.91 mm, and the residual stress level (approximately 270 MPa) is insufficient to ensure high fatigue strength in heavily loaded components. Thus, while the profiled roller improves productivity and surface quality, it is less effective in achieving the required strength characteristics.

This trade-off is effectively resolved by employing a modified cylindrical profile (with S_{cr} = = 2.5 mm). The proposed geometry with fillet transitions enables deformation under conditions of "controlled constraint", thereby combining the advantages of the baseline approaches. With productivity comparable to that of the profiled tool (***N*** = 38 passes), the modified profile achieves a hardening depth of 1.02 mm (only 10% lower than that of the toroidal tool), while maintaining a low microrelief height (h_{res} ≈ ≈ 2.0–5.0 mm) due to the leveling effect of the cylindrical section. A key finding is the transformation of the residual stress distribution from a peak-like profile to a quasi-rectangular form with a stable level of 320 MPa (see Fig. 11, *b*). This indicates the formation of a homogeneous hardened layer ("monolith"), free of localized stress concentrations typical of the toroidal approach and the under-processed regions characteristic of the profiled roller.

A key avenue for future research is the experimental verification of the obtained numerical results, as well as the study of the proposed model's sensitivity to variations in the physical and mechanical properties of the processed materials (including steels with different strength levels). To confirm the adequacy of the developed mathematical model, physical experiments are planned, involving the measurement of residual stresses using X-ray diffractometry and the investigation of the microhardness distribution across the depth of the hardened layer. In addition, the topography and roughness parameters of the processed surfaces will be evaluated using modern profilometry techniques. The obtained results will substantiate the theoretical conclusions and further refine the parameters of the developed finite element model.

Conclusion

Consistent with the objective of this study, and based on numerical simulation and the solution of a bi-criteria optimization problem, the following conclusions can be drawn:

1. A step-by-step analysis established that the optimal geometric parameter for the toroidal profile is R_{pr} = 5.0 mm, and for the profiled roller, R_{pr} = 15.5 mm. It was also found that, despite the theoretical advantages of line contact, the smooth cylindrical profile exhibits a critical drawback – the formation of severe plastic pile-up at the edges (h_p ≈ 37.7 μm) and a highly non-uniform stress field.

2. A comparative evaluation showed that none of the baseline configurations can fully address the technological challenge. The toroidal profile provides a maximum hardening depth (1.15 mm) but exhibits extremely low productivity (***N*** = 188 passes). In contrast, the profiled roller ensures high productivity (***N*** = 31 passes) but fails to generate sufficient contact pressure to achieve the required hardening depth (h_h < 1.0 mm). The smooth cylindrical profile is unsuitable for high-quality processing due to pronounced edge effects.

3. The proposed filleted roller design surpasses the limitations of the baseline schemes by implementing deformation under "controlled constraint" conditions. This approach minimizes the plastic pile-up height from h_p = 37.7 μm to 6.5 μm, allowing an increase in the circular feed step up to S_{cr} = 2.5 mm without compromising the final surface roughness (h_{res} = 2–5 μm). As a result, an optimal balance between productivity and surface integrity is achieved. A hardened layer with a depth of h_h = 1.02 mm is formed, characterized by a uniform ("quasi-rectangular") distribution of compressive residual stresses (300–320 MPa). This is achieved with a productivity nearly five times higher than that of the toroidal scheme.

References

1. Suslov A.G. *Kachestvo poverkhnostnogo sloya detalei mashin* [Quality of the surface layer of machine parts]. Moscow, Mashinostroenie Publ., 2000. 320 p. ISBN 5-217-02976-5.

2. Jawahir I.S., Brinksmeier E., M'Saoubi R., Aspinwall D.K., Outeiro J.C., Meyer D., Umbrello D., Jayal A.D. Surface integrity in material removal processes: Recent advances. *CIRP Annals*, 2011, vol. 60 (2), pp. 603–626. DOI: 10.1016/j.cirp.2011.05.002.

3. Suslov A.G., Bez"yazychnyi V.F., Panfilov Yu.V. *Tekhnologiya i instrumenty otdelochno-uprochnyayushchei obrabotki detalei poverkhnostnym plasticheskim deformirovaniem*. V 2 t. T. 2 [Technology and tools for finishing and strengthening treatment of parts by surface plastic deformation. In 2 vol. Vol. 2]. Moscow, Mashinostroenie Publ., 2014. 444 p. ISBN 978-5-94275-710-6.

4. Çelik Y., Yıldız T. The influence of roller burnishing process parameters on surface quality and fatigue life of AA 7075-T6 alloy. *Material Science & Engineering Technology*, 2022, vol. 53 (5), pp. 608–616. DOI: 10.1002/mawe.202100291.

5. Odintsov L.G. *Uprochnenie i otdelka detalei poverkhnostnym plasticheskim deformirovaniem* [Strengthening and finishing of parts by surface plastic deformation]. Handbook. Moscow, Mashinostroenie Publ., 1987. 328 p.

6. Smelyanskii V.M. *Mekhanika uprochneniya detalei poverkhnostnym plasticheskim deformirovaniem* [Mechanics of hardening of parts by surface plastic deformation]. Moscow, Mashinostroenie Publ., 2002. 300 p. ISBN 5-217-03065-8.

7. Korzynski M. Modeling and experimental validation of the force-surface roughness relation for smoothing friction burnishing with a spherical tool. *International Journal of Machine Tools and Manufacture*, 2007, vol. 47 (12–13), pp. 1956–1964. DOI: 10.1016/j.ijmachtools.2007.03.002.

8. Maximov J.T., Duncheva G.V., Anchev A.P., Ichkova M.D. Slide burnishing – review and prospects. *The International Journal of Advanced Manufacturing Technology*, 2019, vol. 104 (1–4), pp. 785–801. DOI: 10.1007/s00170-019-03881-1.

9. Raza A., Kumar S. A critical review of tool design in burnishing process. *Tribology International*, 2022, vol. 174, p. 107717. DOI: 10.1016/j.triboint.2022.107717.

10. Cui L., He Y. A new logarithmic profile model and optimization design of cylindrical roller bearing. *Industrial Lubrication and Tribology*, 2015, vol. 67 (5), pp. 498–508. DOI: 10.1108/ILT-01-2015-0006.

11. Klocke F., Bäcker V., Wegner H., Feldhaus B., Baron H.U., Hessert R. Influence of process and geometry parameters on the surface layer state after roller burnishing of IN718. *Production Engineering*, 2009, vol. 3 (4–5), pp. 391–399. DOI: 10.1007/s11740-009-0182-0.

12. Halme J., Andersson P. Rolling contact fatigue and wear fundamentals for rolling bearing diagnostics. *Proceedings of the Institution of Mechanical Engineers, Part J: Journal of Engineering Tribology*, 2010, vol. 224 (4), pp. 377–393. DOI: 10.1243/13506501JET656.

13. Hassan A.M. The effects of ball- and roller-burnishing on the surface roughness and hardness of some non-ferrous metals. *Journal of Materials Processing Technology*, 1997, vol. 72 (3), pp. 385–391. DOI: 10.1016/S0924-0136(97)00199-4.

14. Dzierwa A., Markopoulos A.P. Influence of ball-burnishing process on surface topography parameters and tribological properties of hardened steel. *Machines*, 2019, vol. 7 (1), p. 11. DOI: 10.3390/machines7010011.

15. Sanchez L.E.A., Giaretta F., Nogueira L.G., Neto R.I. Effect of hot burnishing aided by infrared radiation on the modification of surface and subsurface of AISI 1045 steel. *Procedia CIRP*, 2017, vol. 58, pp. 463–468. DOI: 10.1016/j.procir.2017.03.254.

16. Zaides S.A., Ngo Cao Cuong. Intensifikatsiya napryazhenno-deformirovannogo sostoyaniya v ochage deformatsii pri stesnennykh usloviyakh nagruzheniya [Stress-strain state intensification in deformation zone under constraint loading conditions]. *Vestnik Irkutskogo gosudarstvennogo tekhnicheskogo universiteta = Proceedings of Irkutsk State Technical University*, 2015, no. 7 (102), pp. 55–59.

17. Duncheva G.V., Maximov J.T., Anchev A.P., Dunchev V.P., Atanasov T.P., Capek J. Finite element and experimental study of the residual stresses in 2024-T3 Al alloy treated via single toroidal roller burnishing. *Journal of the Brazilian Society of Mechanical Sciences and Engineering*, 2021, vol. 43, p. 52. DOI: 10.1007/s40430-020-02775-8.

18. Mohammadi F., Sedaghati R., Bonakdar A. Finite element analysis and design optimization of low plasticity burnishing process. *The International Journal of Advanced Manufacturing Technology*, 2014, vol. 70 (5–8), pp. 1337–1354. DOI: 10.1007/s00170-013-5406-y.

19. Elsamanty M., Youssef W.F., Abdulsalam M., Ibrahim A. Numerical investigation of ball burnishing process using a comprehensive three-dimensional finite element model. *International Journal of Precision Engineering and Manufacturing*, 2025, vol. 27 (2), pp. 529–547. DOI: 10.1007/s12541-025-01372-w.

20. Balland P., Tabourot L., Degre F. Mechanics of the burnishing process. *Precision Engineering*, 2013, vol. 37, pp. 129–134. DOI: 10.1016/j.precisioneng.2012.07.008.

21. Cui P., Liu Z., Yao X., Cai Y. Effect of ball burnishing pressure on surface roughness by low plasticity burnishing Inconel 718 pre-turned surface. *Materials*, 2022, vol. 15 (22), p. 8067. DOI: 10.3390/ma15228067.

22. Ciulli E., Betti A., Forte P. The applicability of the Hertzian formulas to point contacts of spheres and spherical caps. *Lubricants*, 2022, vol. 10 (10), p. 233. DOI: 10.3390/lubricants10100233.

23. Zaides S.A., Le T.Ch. Otsenka vliyaniya napravleniya uprochnennykh armirovannykh volokon na deformiruyushchuyu sposobnost' tsilindricheskikh detalei [Assessment of the reinforced fiber direction influence on

deformability of the cylindrical parts]. *Izvestiya vysshikh uchebnykh zavedenii. Mashinostroenie = BMSTU Journal of Mechanical Engineering*, 2025, no. 9 (786), pp. 41–52.

24. Blyumenstein V.Yu. Mekhanika tekhnologicheskogo nasledovaniya kak nauchnaya osnova proektirovaniya slozhnoprofil'nykh instrumentov dlya uprochnyayushchei obrabotki poverkhnostnym plasticheskim deformirovaniem [Mechanics of technological inheritance as scientific basis of designing complex-profile tools for hardening treatment by surface plastic deformation]. *Naukoemkie tekhnologii v mashinostroenii = Science Intensive Technologies in Mechanical Engineering*, 2017, no. 8, pp. 7–16. DOI: 10.12737/article_5971e6e56cd3d8.31840363.

Conflicts of Interest

The authors declare no conflict of interest.